Nanoscale

PAPER

View Article Online
View Journal | View Issue

Cite this: *Nanoscale*, 2016, **8**, 8138

Biocompatible magnetic core–shell nanocomposites for engineered magnetic tissues†

Laura Rodriguez-Arco,*[a,b] Ismael A. Rodriguez,[b,c] Victor Carriel,[b,c] Ana B. Bonhome-Espinosa,[a,b] Fernando Campos,[b,c] Pavel Kuzhir,[d] Juan D. G. Duran[a,b] and Modesto T. Lopez-Lopez*[a,b]

The inclusion of magnetic nanoparticles into biopolymer matrixes enables the preparation of magnetic field-responsive engineered tissues. Here we describe a synthetic route to prepare biocompatible core–shell nanostructures consisting of a polymeric core and a magnetic shell, which are used for this purpose. We show that using a core–shell architecture is doubly advantageous. First, gravitational settling for core–shell nanocomposites is slower because of the reduction of the composite average density connected to the light polymer core. Second, the magnetic response of core–shell nanocomposites can be tuned by changing the thickness of the magnetic layer. The incorporation of the composites into biopolymer hydrogels containing cells results in magnetic field-responsive engineered tissues whose mechanical properties can be controlled by external magnetic forces. Indeed, we obtain a significant increase of the viscoelastic moduli of the engineered tissues when exposed to an external magnetic field. Because the composites are functionalized with polyethylene glycol, the prepared bio-artificial tissue-like constructs also display excellent *ex vivo* cell viability and proliferation. When implanted *in vivo*, the engineered tissues show good biocompatibility and outstanding interaction with the host tissue. Actually, they only cause a localized transitory inflammatory reaction at the implantation site, without any effect on other organs. Altogether, our results suggest that the inclusion of magnetic core–shell nanocomposites into biomaterials would enable tissue engineering of artificial substitutes whose mechanical properties could be tuned to match those of the potential target tissue. In a wider perspective, the good biocompatibility and magnetic behavior of the composites could be beneficial for many other applications.

Received 10th January 2016,
Accepted 10th March 2016

DOI: 10.1039/c6nr00224b

www.rsc.org/nanoscale

Introduction

The assembly of nanoparticles of different materials in hybrid core–shell nanostructures has become increasingly attractive in recent years. Such nano-platforms aim to integrate the specific characteristics of each material into a single, multifunctional entity, capable of delivering a wide range of features.[1,2] Potential applications of core–shell composites comprise heterogeneous catalysis, energy conversion, water remediation, optoelectronics and biomedical applications.[2–5]

In the particular case of biomedical applications, a precise temporospatial control of the nanocomposites in a minimally invasive way is tremendously advantageous. In this regard, magnetic nanoparticles (MNPs) can be integrated into the nanostructures to provide this feature, located either at the core of the core–shell architecture or forming the external shell.[6,7] Because of their magnetic nature, MNPs can be guided by non-contact forces (*i.e.*, external magnetic field gradients), and allow, at the same time, *in situ* monitoring by magnetic resonance imaging (MRI) or computerized axial tomography scanning (CT). Furthermore, their particulate character and high surface area make it possible to bind molecules such as tissue or tumor-specific antibodies, drugs, diagnostic molecules, growth factors, peptides, *etc.*[7–9] As for tissue engineering applications, MNPs have been previously dispersed in biopolymer matrixes to synthesize innovative artificial magnetic scaffolds without affecting cell adhesion, proliferation or differentiation.[10–26] Such artificial tissues also possess the unique feature of being effectively magnetized by the application of external fields, and thus, they may attract functionalized MNPs carrying growth factors, drugs or cells.[11,17,22]

[a]*Department of Applied Physics, University of Granada, Faculty of Science, Campus de Fuentenueva, 18071 Granada, Spain. E-mail: l_rodriguezarco@ugr.es, modesto@ugr.es*
[b]*Instituto de Investigación Biosanitaria ibs.GRANADA, Granada, Spain*
[c]*Department of Histology (Tissue Engineering Group), University of Granada, Faculty of Medicine, Avenida de la Investigación, 11, 18016 Granada, Spain*
[d]*Laboratory of Condensed Matter Physics, UMR No. 7336, University of Nice–Sophia Antipolis, CNRS, 28 Avenue Joseph Vallot, 06100 Nice, France*
†Electronic supplementary information (ESI) available. See DOI: 10.1039/c6nr00224b

In all these previous studies reporting magnetic scaffolds, the size of the MNPs was around 10 nm. Nevertheless, the use of MNPs larger than 50–100 nm has additional advantages from the magnetic point of view, because the magnetic interaction energy between large MNPs dominates over Brownian motion.[27] Actually, the mechanical properties of dispersions of large MNPs typically used in materials science (*e.g.*, suspensions, gels, foams) can be changed in a reversible way by the application of an external magnetic field.[27–29] In a recent work we have explored such a phenomenon in the case of novel magnetic substitutes generated by tissue engineering consisting of solid MNPs of around 100 nm, to show that it is possible to tune, in a reversible way, their mechanical response by external magnetic forces.[30]

However, the colloidal stability of large magnetic particles is usually rather poor because they tend to settle due to gravitational forces. Such a problem may be partially overcome if magnetic core–shell nanocomposites are employed instead. Indeed, if the material of the core has low density (*e.g.*, polymeric core), gravitational settling is much slower because of the reduction of the composite average density. In addition, the distribution of the MNPs around a non-magnetic core also has advantages in terms of the magnetic response of the composite particle. Indeed, in a previous study we have shown that for a given volume fraction of magnetic material, such a distribution leads to higher magnetic susceptibility at low to medium magnetic fields than in the case of solid particles, which means stronger responses to external fields.[31]

In this work we report new biocompatible magnetic core–shell nanostructures (diameter ~500 nm) which are tested for the generation of magnetic bio-artificial tissue-like constructs. These nanocomposites consist of a polymeric core and a shell of MNPs. In addition, biocompatibility is achieved by an additional layer of polyethylene glycol. We characterize the composites from the physicochemical point of view (morphology, composition and magnetic properties) and compare them with solid particles (*i.e.*, no core–shell structure). We also analyze their *ex vivo* and *in vivo* biocompatibility and use them to generate engineered magnetic tissues, which also exhibit an active cell proliferation and good *in vivo* biocompatibility. We finally evaluate the mechanical properties of the prepared engineered tissues and test if it is possible to tune them by the application of external magnetic fields. In addition, we compare the mechanical properties with those of the engineered tissues prepared with solid particles of our previous work,[30] to show that using a core–shell architecture is highly advantageous to obtain stronger magnetic field-responsiveness in these novel biomaterials.

Results and discussion

Synthesis and characterization of magnetic nanocomposites

We prepared biocompatible magnetic core–shell composites following a two-step procedure as schematized in Fig. 1: (i) *in situ* deposition of MNPs around a polymer core (Poly@Mag composites), and (ii) coating of the resulting nanostructures with polyethylene glycol (PEG), which was used to impart to them the necessary biocompatibility to be incorporated into bio-artificial tissue-like constructs (Poly@Mag@PEG composites). Indeed, coating nanoparticles with a PEG layer reduces the attack by macrophages as shown in previous studies.[32–34] The composite cores were copolymer spheres of acrylic monomers functionalized with carboxylic, COOH groups (Poly). We first dispersed the cores in water at pH ~ 10 to promote deprotonation of COOH and therefore, to generate negative surface charge. We then added Fe^{2+} and Fe^{3+} solutions (molar ratio $[Fe^{3+}]/Fe^{2+}] = 0.5$). Because of their opposite charge, Fe^{2+} and Fe^{3+} cations were electrostatically attracted to the core surface. Once adsorbed, we used an alkali solution to induce co-precipitation of iron oxide MNPs (a black precipitate appeared). For PEG coating we adapted the method proposed in ref. 35, which is based on the formation of an emulsion. We labelled these composites as Poly@Mag@PEG.

Stage (i) of the synthetic procedure resulted in the polymer cores fully and homogeneously coated with MNPs. More specifically, the smooth surface of the core (Fig. 2a and b) appeared completely covered with MNPs of a diameter of 10–50 nm as shown by scanning (SEM) and transmission (TEM) electron microscopy (see Fig. 2c and S1 of the ESI,† and 2d respectively). Energy-dispersive X-ray spectroscopy (EDX) revealed iron as the predominant material of the outer shell (not shown). The Fourier transform infrared spectroscopy (FTIR) spectra of Poly@Mag composites also exhibited the

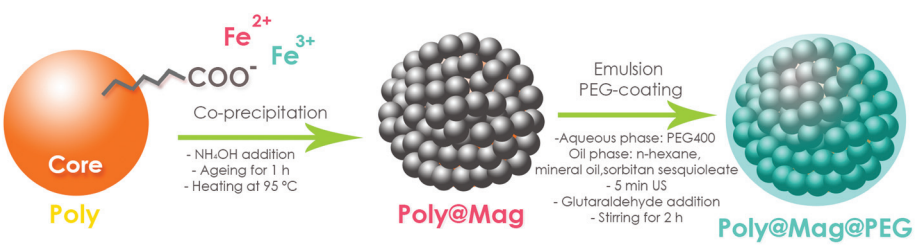

Fig. 1 Sketch of the procedure for magnetic core–shell nanostructure synthesis. In a first step, spheres of acrylic copolymers functionalized with COO^- groups (Poly) were used as cores for electrostatic adsorption of Fe^{2+} and Fe^{3+} cations, and subsequent surface deposition of MNPs *via* co-precipitation under alkaline conditions. The resulting nanocomposites (Poly@Mag) were covered with polyethylene glycol (PEG) in a second step, using a previous procedure[35] based on emulsion formation and yielding Poly@Mag@PEG composites.

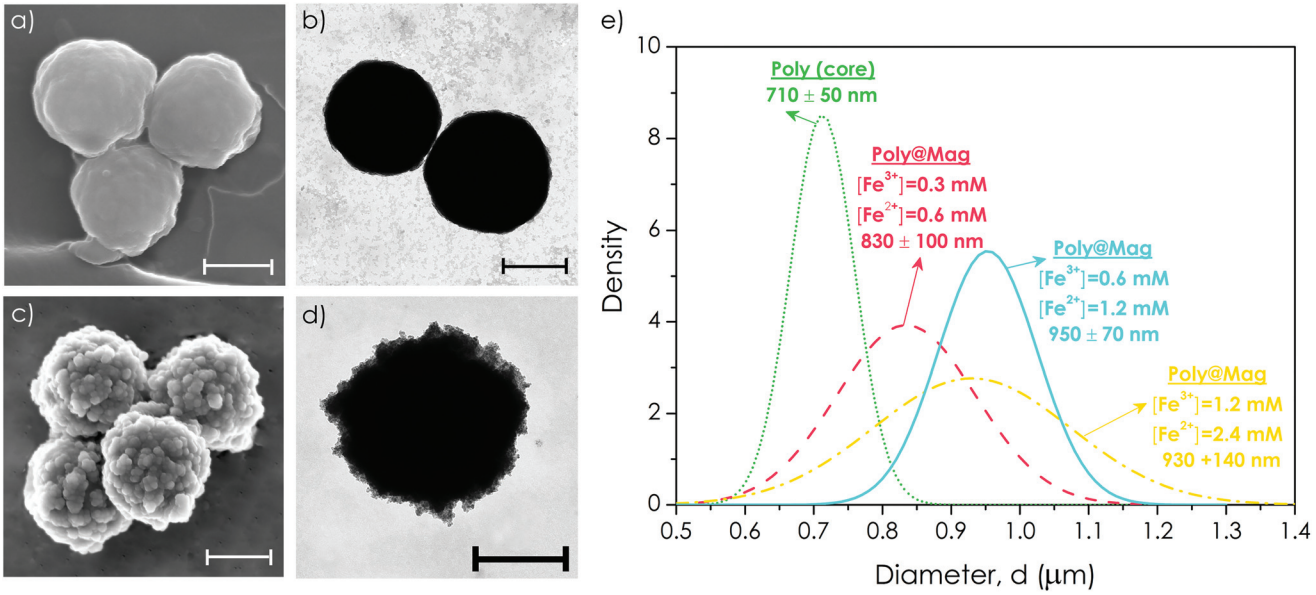

Fig. 2 Size and morphology of Poly@Mag composites. Scanning (a and c) and transmission (b and d) electron microscopy photographs of the polymer core, Poly (a and b), and of Poly@Mag (c and d) composites (bar length = 500 nm). As observed, the cores appeared fully coated with MNPs of around 10–50 nm diameter. (e) Size distribution of Poly particles and Poly@Mag composites for different concentrations of iron precursors. In general, higher concentrations of precursors yielded thicker MNP coatings.

characteristic Fe–O band at 590–630 cm^{-1} confirming the presence of iron oxide in the nanocomposites (see Fig. S2 of the ESI†).[36] Similarly, thermogravimetric analysis (TGA) showed a residual weight of inorganic material at high temperature associated with the MNPs of the shell (see Fig. S3 of the ESI†).

The obtained core–shell structures were uniform in size. The average diameter varied depending on the employed concentration of iron precursors with respect to polymer cores: higher concentrations of precursors yielded thicker MNP coatings. For example, doubling the concentration of iron cations from $[Fe^{3+}]$ = 0.3 mM and $[Fe^{2+}]$ = 0.6 mM to $[Fe^{3+}]$ = 0.6 mM and $[Fe^{2+}]$ = 1.2 mM resulted in an increase of Poly@Mag diameter from 830 ± 100 nm to 950 ± 70 nm (Fig. 2e). This result confirms the possibility of tuning the thickness of the magnetic shell, as shown in previous studies.[37,38] However, a further double increase of the concentration did not yield a higher diameter, but a rather broader size distribution (Fig. 2e).

The synthesized composites were ferromagnetic with a tunable response to the external magnetic field. The co-precipitation reaction yielded magnetite (Fe_3O_4), which likely oxidized to maghemite (γ-Fe_2O_3) in the presence of oxygen,[39] because the X-ray diffraction (XRD) spectrum of the nanocomposites could be fitted by both patterns (see Fig. S4 of the ESI†). The saturation magnetization of γ-Fe_2O_3 and Fe_3O_4 is similar (380 and 480 kA m^{-1} respectively).[40] The saturation magnetization of our composites was as high as M_s = 150 kA m^{-1} for the samples with a higher content of the magnetic material (40 vol%) (Fig. 3a). The magnetization curves were reversible with almost negligible values of coercivity, remanence, or hysteresis, suggesting nearly superparamagnetic behaviour (Fig. 3a).

However, the most significant advantage of using core–shell nanostructures with respect to solid magnetic particles is the possibility of customizing the initial magnetic susceptibility of the particles (χ_i) by changing the thickness of the magnetic shell. Actually, classical electromagnetism predicts higher χ_i as the thickness of the shell becomes thinner, for a given amount of magnetic material.[41,42] To test this for our nanocomposites we first normalized the magnetization of the samples by dividing it by the saturation magnetization (*i.e.*, M/M_s), so we could compare them in conditions of an equal concentration of the magnetic material. We then plotted this normalized magnetization against the magnetic field and compared the initial slope of the curves, (*i.e.*, the magnetic susceptibility). We confirmed that composites with smaller diameters (*i.e.*, thinner magnetic shells) showed higher χ_i (Fig. 3b). Furthermore, the susceptibilities at low to medium fields of the core–shell nanostructures were always higher than the susceptibility of solid magnetite particles of diameter of the same order of magnitude, previously prepared in our group[43] (Fig. 3b).

In addition to higher χ_i, our nanocomposites showed better stability against gravitational settling than solid particles. Indeed, for Poly@Mag samples, the absorbance (A) was reduced because of settling to a third of its initial value (A_0) only after 24 h. For solid magnetite nanoparticles of similar size, such a reduction of absorbance took place in less than 1 h (see Fig. 3c).[44] Such a better colloidal stability for our nanocomposites was due to their lower average density because of the lighter polymer core (density ~1 g cm^{-3}). This feature is highly advantageous for biomedical applications (*e.g.*, prepa-

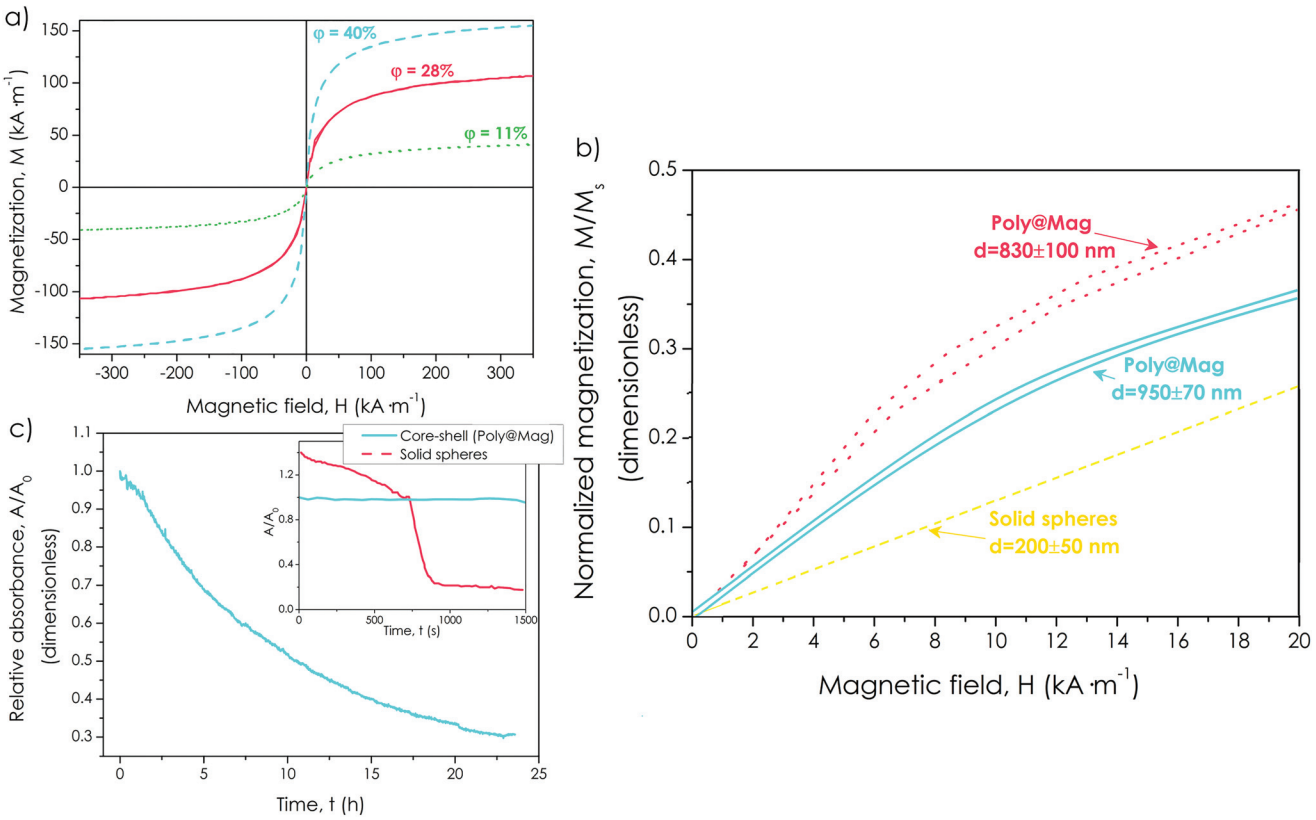

Fig. 3 Special features of magnetic core–shell nanostructures. (a) Magnetization, *M*, plotted against the magnetic field, *H*, for core–shell composites with different concentrations of the magnetic material, ϕ (indicated). As observed, samples with higher magnetic contents displayed higher values of the saturation magnetization. (b) Normalized magnetization (M/M_s) *vs.* the magnetic field, *H*, for core–shell nanocomposites of different diameters (indicated). Thicker magnetic coatings gave rise to lower values of the magnetic susceptibility at low-medium fields (slope of the curve). The susceptibility for solid magnetite nanoparticles with diameter of the same order of magnitude was even lower (reprinted from S. A. Gómez-Lopera, R. C. Plaza and A. V. Delgado, Synthesis and Characterization of Spherical Magnetite/Biodegradable Polymer Composite Particles, *J. Colloid Interface Sci.*, **240**, 40–47, Copyright (2001), with permission from Elsevier[43]). (c) Absorbance at 550 nm, *A*, normalized by the value at the beginning of the test, A_0, as a function of time for core–shell nanocomposites and for solid particles (adapted with permission from S. A. Gómez-Lopera, J. L. Arias, V. Gallardo and A. V. Delgado, *Langmuir*, 2006, **22**, 2816. Copyright (2006) American Chemical Society[44]). A significant reduction of the absorbance (*i.e.*, A/A_0 = 0.3) was only obtained after 24 h for the core–shell structures, in comparison with the fast reduction observed for solid particles.

ration of magnetic artificial tissues), for which a good dispersion of the magnetic composites in the continuous medium is essential.

The magnetic nanostructures were successfully coated with PEG (stage (ii) in the sketch of Fig. 1), showing excellent chemical stability and biocompatibility. The successful PEG coating was evidenced by the appearance of new bands in the FTIR spectra corresponding to the in-plane C–H and O–H deformations and of the combination bands of O–C–H and C–O–H (see Fig. S2 of the ESI†). It also gave rise to an additional loss of weight in comparison with Poly@Mag composites in TGA (see Fig. S3 of the ESI†). The PEG shell appeared as a translucent thin film (thickness of a few nanometers) around the magnetic shell in TEM images (Fig. 4a and S5 of the ESI†). In spite of its small thickness, the PEG layer protected the magnetic core from mild acidic attack. Actually, Poly@Mag nanospheres lost their magnetic character after immersion in HCl (0.1 M) for 7 days (Fig. 4b), while Poly@Mag@PEG composites were not significantly affected (Fig. 4c). In addition to better chemical stability, the PEG coating improved the biocompatibility of the composites. Human gingival fibroblasts cultured in the presence of Poly@Mag composites showed substantial morphology alterations. While some of them maintained the typical elongated spindle shape of fibroblasts, others appeared to have a more irregular and rounded morphology (Fig. 4f). These latter results were similar but not comparable to those observed in the negative control group of cells cultured in the presence of malign agents (Fig. 4e). Actually, quantitative analysis of DNA release showed no significant differences ($p > 0.05$) for the Poly@Mag group as compared to the positive control group (cells growth under normal conditions) (Fig. 4h). These results suggested that Poly@Mag composites just altered cell attachment to the culture flask, but not the cell membrane permeability (cytoplasmic and nuclear), which evidenced the absence of irreversible cell damage. Interestingly, the WST-1 cell viability assay revealed significant differences ($p < 0.05$) in the cells exposed to Poly@Mag as compared to the positive

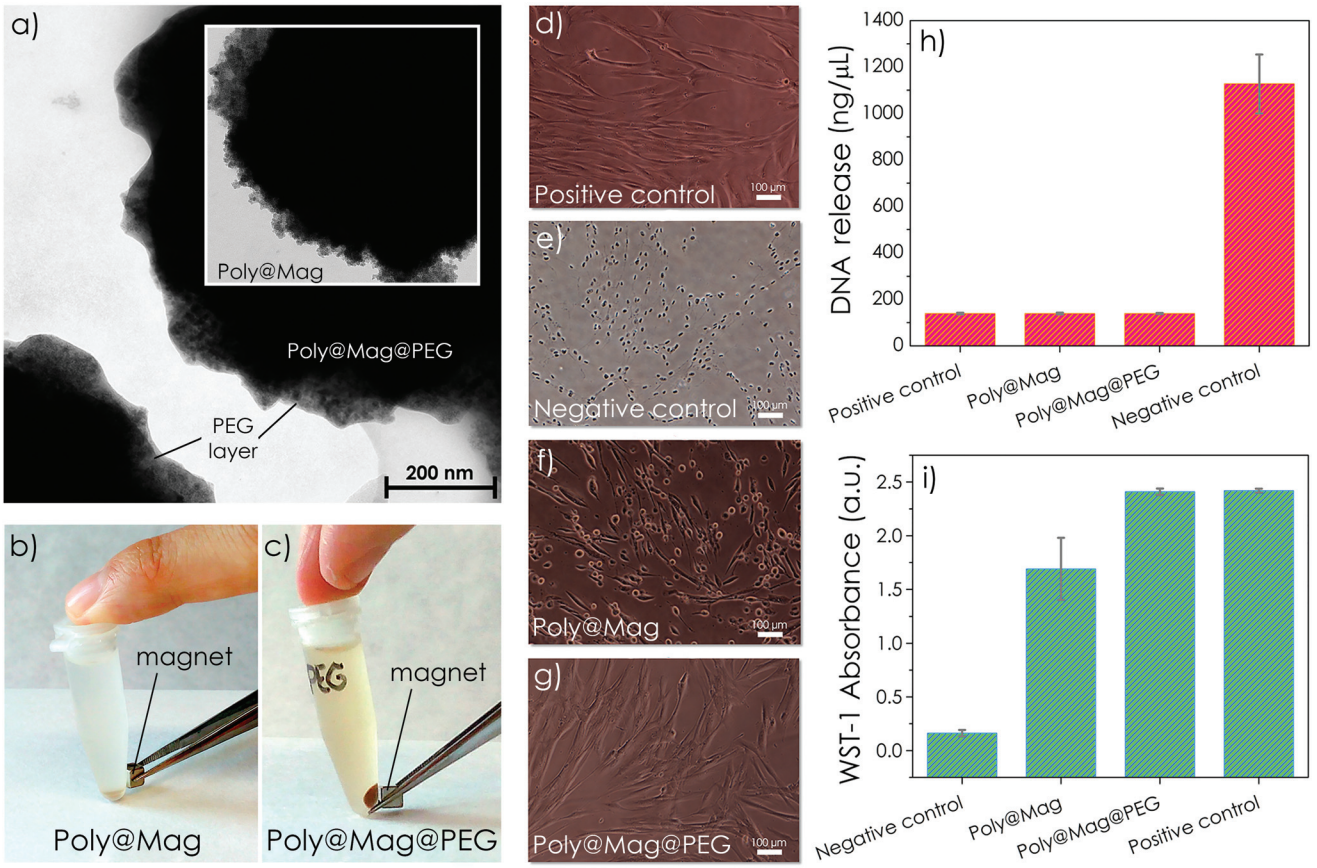

Fig. 4 Characterization of Poly@Mag@PEG composites. (a) Transmission electron microscopy picture of Poly@Mag@PEG composites. The PEG coating appeared as a translucent thin film around the magnetic shell in contrast to Poly@Mag composites with no PEG coating (inset). (b and c) Macroscopic appearance of samples of Poly@Mag (b) and Poly@Mag@PEG (c) composites after 7 days of acid treatment. Poly@Mag@PEG composites remained magnetic because of the protective PEG layer. (d–g) Microscopy images of fibroblasts. Those cultured in the presence of Poly@Mag@PEG composites (g) showed an elongated shape identical to the shape of the fibroblasts of the positive control (d). For Poly@Mag composites (f), some cells preserved the spindle shape, while others appeared more rounded like those of the negative control (e). (h) Quantification of DNA release after disintegration of the nuclear membrane. The core–shell nanocomposites (Poly@Mag and Poly@Mag@PEG) showed no significant differences with respect to the positive control. (i) Cell cytotoxicity results (WST-1 test). Samples with a greater number of viable cells displayed stronger absorbance at 450–690 nm because of the formation of formazan. The number of viable cells was therefore smaller for Poly@Mag composites than for the positive control, while it remained approximately the same for Poly@Mag@PEG composites.

control group (Fig. 4i). However, both quantitative analyses (DNA analysis and WST-1) showed no significant differences ($p > 0.05$) between the fibroblasts cultured in the presence of Poly@Mag@PEG particles and those cultured under normal conditions, *i.e.* positive control (Fig. 4h and i). Actually, these cells preserved the elongated morphology (Fig. 4g) and were almost identical to those of the positive control sample of natural proliferation (Fig. 4d). These results support the high *ex vivo* biocompatibility associated with the PEG coating, which makes Poly@Mag@PEG composites excellent candidates to be included in engineered tissue substitutes.

Preparation and characterization of magnetic tissue substitutes

We successfully incorporated Poly@Mag@PEG composites into fibrin-agarose (FA) hydrogels containing human oral mucosa fibroblasts to obtain magnetic field-responsive tissue substitutes.

Fibrin is a natural polymer frequently used in tissue engineering. Combined with agarose, the biomechanical properties of the resulting engineered tissues are considerably enhanced and match the mechanical response of several native soft human tissues.[45–47] Furthermore, fibrin-agarose matrixes have been successfully employed to generate substitutes of human tissues such as the cornea, oral mucosa, skin and peripheral nerves, which proved to be effective *in vivo*.[45,46,48] In our case, the core–shell nanocomposites appeared homogeneously distributed over the network of fibrin fibers as shown by SEM images (Fig. 5a). Interestingly, they frequently acted as connectors between the fibrin fibers (see the inset of Fig. 5a). Very likely, the negatively charged Poly@Mag@PEG nanocomposites at physiological pH (zeta potential of −37.1 ± 0.8 mV at pH = 7.4) attracted the positively charged E domains of fibrin

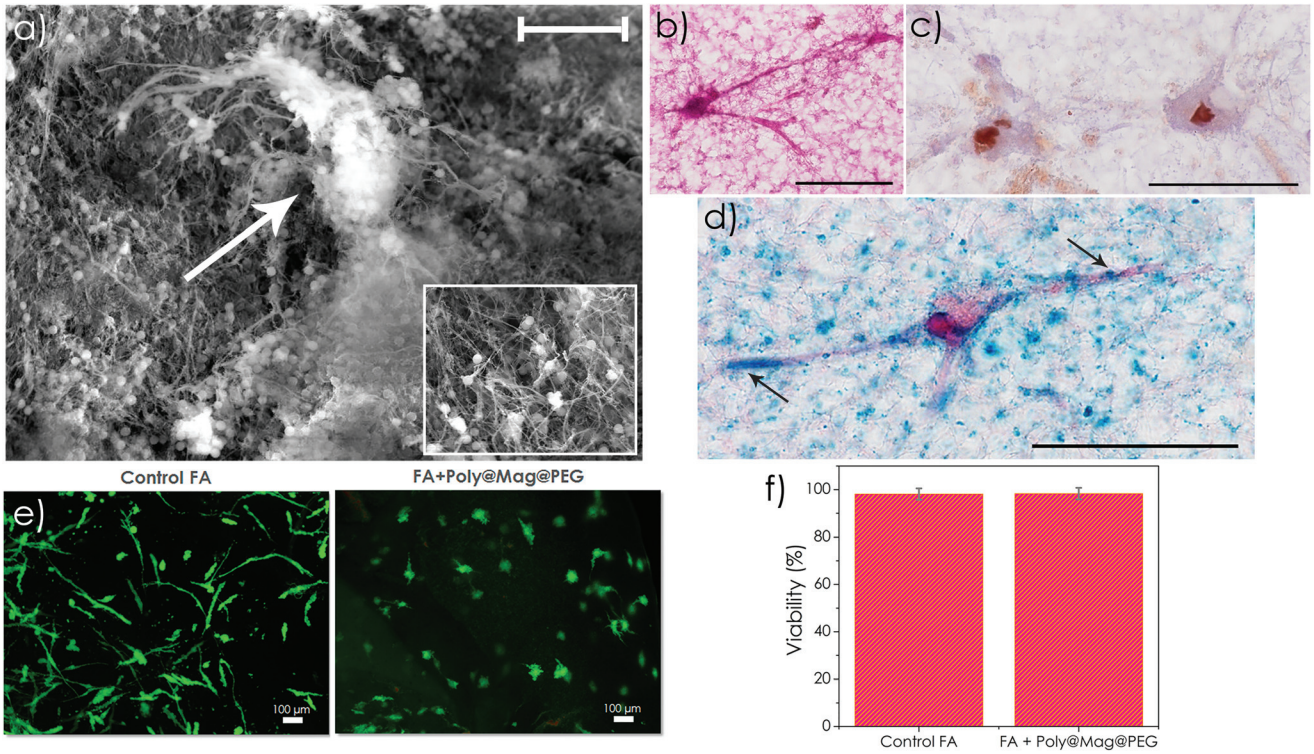

Fig. 5 Characterization of magnetic tissue substitutes. (a) Scanning electron microscopy of fibrin-agarose (FA) engineered tissue with Poly@Mag@PEG nanostructures (bar length = 10 μm). As observed, the particles were homogeneously distributed over the network of fibrin fibres and the cells maintained their orthotopic shape (the cell is indicated with an arrow). The insets allow better observation of the connection between the nanocomposites and fibrin fibres. (b–d) *Ex vivo* histological analysis of the magnetic tissues. H&E staining showed that the fibroblasts were able to acquire their typical elongated shape with prominent nuclei in the presence of the nanocomposites (b). PCNA immunohistochemical analysis showed proliferating fibroblasts (c) and Perl's histochemical method specifically stained in blue the Poly@Mag@PEG composites. Black arrows indicate the large filopodia of the fibroblasts which interacted with some nanocomposites stained in blue (d). Scale bar = 5 μm. (e) Live/Dead™ fluorescence microscopy images of a control artificial tissue of FA without nanocomposites (left image in (e)) and an engineered tissue with Poly@Mag@PEG composites (right image in (e)). Fluorescent green color corresponds to live cells. Both samples exhibited identical appearance, with no dead cells (red color). Scale bar = 100 μm. (f) Quantification of viable cells by the Live/Dead™ technique. There were no significant differences in the percentage of viable cells between the sample with Poly@Mag@PEG particles and the FA control sample.

monomers (generated after thrombin cleavage of the fibrinopeptides of fibrinogen).[49] The oxygen atoms of the PEG layer, which can play the role of hydrogen bond acceptors,[50] may have formed hydrogen bonds with the hydrogen bond donors of fibrin monomers. As a result, fibrin monomers anchored on Poly@Mag@PEG composites, which acted as condensation sites for the subsequent polymerization of fibrin fibers. However, future investigations are needed to confirm these hypotheses.

Cell morphology and proliferation in the magnetic tissue-like constructs were normal as shown by histological analyses. The engineered tissues with H&E showed a random distribution of fibroblasts in the FA matrix (see Fig. 5b and S6 of the ESI†). Interestingly, fibroblasts were found alone or forming small cell clusters (see Fig. S6 of the ESI†), with prominent nuclei in both cases. The nuclei of both individual and cluster-forming fibroblasts showed intense positive immunoreaction for PCNA immunohistochemical analysis (see Fig. 5c and S6 of the ESI†), which confirmed the active proliferation of fibroblasts in the magnetic tissue substitutes. Fibroblasts preserved their characteristic orthotopic elongated shape with large *filopodia* along the fibrin fibers as shown by SEM (Fig. 5a) and by histological analyses (Fig. 5b–d and S6 of the ESI†), indicating cell-biomaterial interactions. Although homogeneously distributed over the biopolymer, Poly@Mag@PEG composites were frequently observed near the cell surface, around the perinuclear cytoplasm and the large filopodia of the fibroblasts as shown by the intense Prussian blue color of the composites after staining with Perls' histochemical method (see Fig. 5d and S6 of the ESI†). *Ex vivo* Live/Dead™ assays revealed a high number of metabolically active cells in the engineered tissues containing Poly@Mag@PEG composites, which was similar to the values observed for the fibrin-agarose control group (cellular construct without composites). In both cases, fluorescence microscopy only showed live, green-stained, cells (dead cells are stained with red color in this technique) as shown in Fig. 5e. Remarkably, there were no statistically significant differences ($p > 0.05$) between cell viability in the artificial tissues prepared with Poly@Mag@PEG composites (98.3 ± 2.4%) and the fibrin-agarose control (98.1 ± 2.4%) (Fig. 5f),

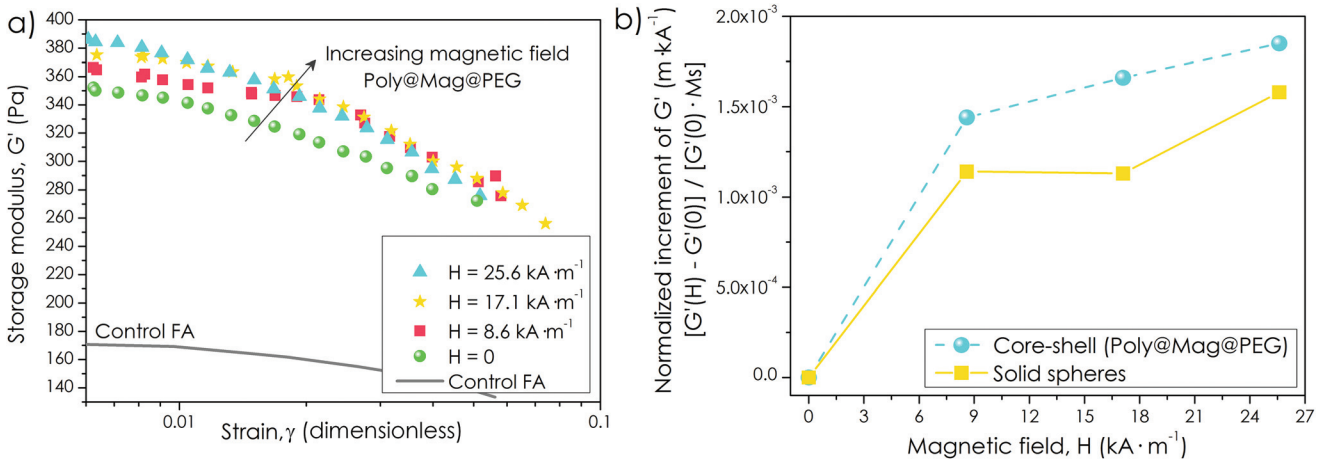

Fig. 6 Mechanical properties of magnetic tissue substitutes. (a) Storage modulus, G', as a function of the amplitude of the oscillatory strain for four values of the applied magnetic field, H (indicated). The mechanical strength of the engineered tissue increased with the magnetic field as evidenced by the increase of G'. (b) Normalization of the relative increment of G' with the field, $[G'(H) - G'(0)]/G'(0)$, by the saturation magnetization of the nanocomposites, M_s for engineered tissues consisting of Poly@Mag@PEG composites and solid magnetic particles of similar size (adapted from M. T. Lopez-Lopez, G. Scionti, A. C. Oliveira, J. D. G. Duran, A. Campos, M. Alaminos and I. A. Rodriguez, *PLoS One*, 2015, **10**, e0133878[30]). As observed, the increment with the field is higher for core–shell nanostructures as a result of the enhancement of the initial magnetic susceptibility observed in Fig. 3.

which demonstrated the high *ex vivo* biocompatibility of Poly@Mag@PEG nanocomposites (Fig. 5f).

The incorporation of magnetic nanocomposites into the artificial tissues transformed them into magnetic field-responsive engineered tissues. Indeed, the engineered tissues prepared with magnetic composites moved when exposed to the magnetic field gradient created by a magnet (see Video 1 of the ESI†). From magnetization measurements (see Fig. S7 of the ESI†) we estimated the volume fraction of the magnetic material in the engineered tissues, which turned out to be ~0.3 vol%. Such a magnetized state of the engineered tissue would allow attraction of functionalized MNPs carrying growth factors, drugs or cells.[11,17,22]

In addition to field-responsiveness, the engineered tissues showed magnetic field-tunable mechanical properties. More specifically, we measured an increase of the storage modulus (G') of the engineered tissue of ~10% when the intensity of the external field was increased from 0 to 25.6 kA m^{-1} (Fig. 6a). G' is connected to the elastic, solid-like, response of the biomaterial when subjected to an oscillatory mechanical stimulus, and therefore, is a measure of its mechanical strength.[51] Furthermore, the sole presence of the nanocomposites in the fibrin network already increased the engineered tissue mechanical strength, even without magnetic field application. Actually, we observed a twofold increase of G' for Poly@Mag@PEG engineered tissues with respect to the FA control at zero field (Fig. 6a). Such an increase was much higher than the one predicted by the classical theory of mechanics of composite materials for a continuous matrix with spherical, completely rigid inclusions,[52] and could only be explained by microstructural changes in the pattern of the fibrin-agarose network due to the Poly@Mag@PEG nanocomposites. As seen in Fig. 5a and d, Poly@Mag@PEG composites were homogeneously distributed around the fibrin network and acted as connectors between the fibrin fibers. This may have enhanced adhesion between fibers and have had a failure retardation effect which could explain the higher values of G' even in the absence of a field.[53] Similar increases with the field were obtained for the loss modulus, G'', related to the dissipation of energy upon the oscillatory mechanical stimulus (see Fig. S8 of the ESI†).[51] The increase of the viscoelastic moduli with the magnetic field was maintained over a broad range of frequencies of the oscillatory strain (see Fig. S9 of the ESI†). Although not huge, such an increase proves that it is possible to control the mechanical behavior of these artificial tissues by the application of an external field. Stronger magnetic fields or higher composite loadings would give rise to stronger mechanical changes.

However, the most interesting result here was the significant enhancement of the mechanical properties when using core–shell magnetic nanostructures in comparison with the solid magnetic particles of similar size reported in ref. 30. Indeed, a normalization of the field-induced increase of G' by the engineered tissue magnetic content, revealed a stronger magnetic response for Poly@Mag@PEG nanocomposites (Fig. 6b). Such an enhancement would be connected to the improvement of the magnetic susceptibility in core–shell nanostructures observed in Fig. 3. This latter result confirms the excellent suitability of these composites to be used in the preparation of novel magnetic tissue substitutes.

Time-dependent *in vivo* biocompatibility of Poly@Mag@PEG composites and magnetic substitutes

We studied the time-dependent *in vivo* biocompatibility of *free* (*i.e.*, in suspension) Poly@Mag@PEG nanocomposites and of

the magnetic tissue-like constructs in the subcutaneous connective tissue of the interscapular region of mice. The free composites were suspended in physiological solution and were carefully injected. The magnetic constructs were surgically implanted. None of the animals died after 21 days in any of the experimental groups. After 21 days the animals showed no signs of side effects and the changes of body weight were similar to those of the control animals.

The subcutaneously injected Poly@Mag@PEG nanocomposites remained in the interscapulum during the duration of the experiment (*i.e.*, 21 days), without migration to the distal organs of the body. The injected nanocomposites formed an irregular and dense mass consisting of nanocomposite aggregates (Fig. 7b–g). The host response around this mass was a moderate acute inflammatory reaction mainly composed of neutrophils, some mononuclear cells and predominantly macrophages (Fig. 7b–g). The inflammatory reaction was more evident after the first week, but it progressively decreased from the second to the third weeks. The inflammatory response was only localized around the region where Poly@Mag@PEG composites were injected. Cells progressively reabsorbed the mass starting from the external part to the inner part. Perls' staining confirmed the presence of phagosomes with Poly@Mag@PEG composites inside the macrophages (Fig. 7d and f) and the picrosirius method revealed a progressive encapsulation of the composite mass by a collagen-rich extracellular matrix and a blood vessel network (Fig. 7c and e). The mass was not fully reabsorbed after 21 days. The histological and histochemical analyses of the liver, kidney, spleen and lungs did not show any inflammatory reaction. There were no macrophages with Poly@Mag@PEG composites inside either. Indeed, all organs were histologically normal during the 21 day follow-up period (Fig. 7n–q). Tissue samples taken from these organs did not exhibit any magnetic response, in contrast to the samples obtained from the interscapular region, which were magnetic because of the presence of the nanocomposites (see Table S1 of the ESI†).

The histological analysis of the magnetic tissue-like constructs evidenced their successful subcutaneous implantation. The constructs showed a regular and compacted morphology (Fig. 7h–m). The nanocomposites appeared homogeneously distributed over the thin FA hydrogel network, either individually or forming small aggregates, in contrast to the bigger aggregates found when the nanocomposites were injected in suspension (insets in Fig. 7c and i respectively). Therefore, the FA hydrogel prevented from the aggregation of the nanocomposites and favored their consistent and homogeneous individual distribution. The use of the FA hydrogel also eased the interaction with the host tissue: host cells were able to invade the implanted constructs from the first week (Fig. 7i and inset), in contrast to the few cells observed in the case of the injected nanocomposite suspension (Fig. 7c and inset). The constructs were not fully reabsorbed after 21 days. The host response to the constructs was a mild to moderate acute inflammatory reaction which progressively decreased over time (Fig. 7h–m). As in the case of the suspension of Poly@Mag@PEG composites, a thin connective tissue capsule composed of collagen fibers and a vascular network was formed around the implants (Fig. 7k and m). The moderate local acute inflammatory reaction did not affect the surrounding connective tissues and distal organs (Fig. 7h–m and r–u). Similarly to what happened to the nanocomposites in suspension, only the samples from the interscapulum showed a magnetic response (see Table S1 of the ESI†), which indicated no migration of the

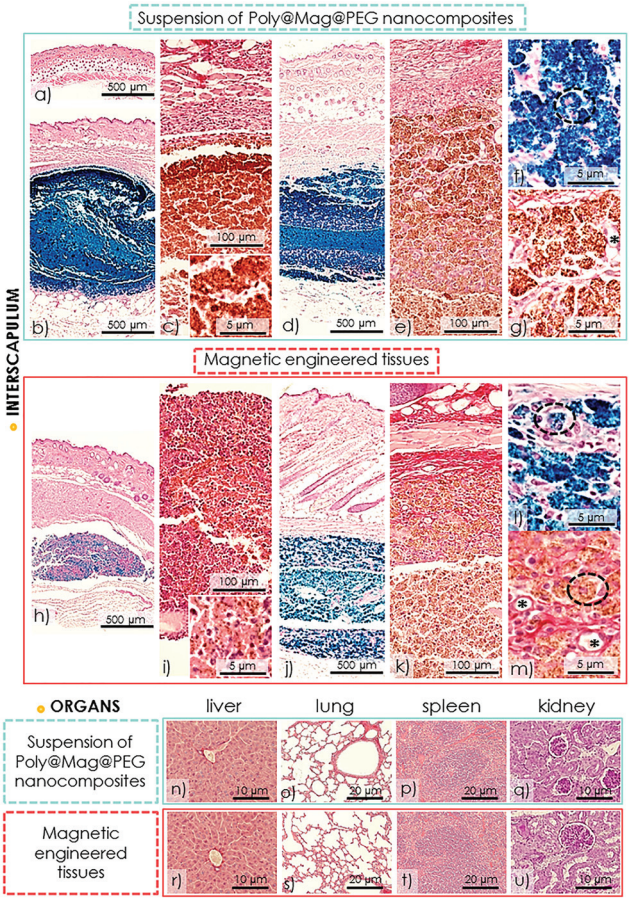

Fig. 7 *In vivo* histological analyses. (a) Native skin control with normal epidermis, dermis and hypodermis. (b–g) Tissue from the interscapulum where Poly@Mag@PEG nanocomposites were injected after 1 week (b and c) and 3 weeks (d–g) post injection. (h–m) Tissue from the interscapulum where the magnetic tissue-like constructs were implanted after 1 week (h and i) and 3 weeks (j–m) post-surgical implantation. (b), (d), (f), (h), (j) and (l) images show the Prussian blue histochemical reaction for the Poly@Mag@PEG nanocomposites (Perl's method). (c), (e), (g), (i), (k) and (m) show picrosirius staining. (e) and (k) show the zone of external degradation and capsule (stained in red with picrosirius). Note the high number of cells in the magnetic engineered tissue after the first week (i and inset) in contrast with the injected nanocomposites (c and the inset). Circles indicate macrophages with nanocomposites, and (*) show small blood vessels in the newly-formed inflammatory capsule after 3 weeks post *in vivo* implantation. (n–u) Tissues from distal organs (liver, lung, spleen and kidney) of the experimental groups of injected Poly@Mag@PEG nanocomposites (n–q) and the implanted magnetic constructs (r–u) after 3 weeks. All organs were histologically normal during the 21 day follow-up period.

Poly@Mag@PEG composites to other organs during the duration of the experiment.

Conclusions

In this work we have synthesized magnetic core–shell nanostructures consisting of a polymeric (acrylic) core, a first shell of magnetic iron oxide nanoparticles, and an additional layer of polyethylene glycol (PEG). These composites have been prepared with the aim of being used as the magnetic phase in novel magnetic field-responsive tissue substitutes.

The prepared composites were uniform in size, the thickness of the magnetic shell increasing with the concentration of iron precursors in the co-precipitation reaction, which allowed tuning of the magnetic properties. The core–shell architecture improved the magnetic response of the composites with respect to solid magnetic particles of similar size. More specifically, the magnetic susceptibility at low to medium fields was higher, and increased when the magnetic shell became thinner. In addition to enhanced magnetic properties, core–shell nanocomposites exhibited remarkably good stability against gravitational settling because of the lower density of the polymer core.

Because of the PEG outer layer, the nanocomposites exhibited excellent chemical stability and biocompatibility (*i.e.*, no significant cell damage and good cell growth and attachment). For this reason, the composites were successfully loaded into fibrin-agarose hydrogels containing human oral mucosa fibroblasts to obtain magnetic field-responsive engineered tissues with metabolically active cells. The fibrin-agarose matrix promoted the interaction with the host tissue when the magnetic tissue-like constructs were implanted *in vivo*. It also prevented colloidal aggregation of the nanocomposites, in contrast to the situation when the nanocomposites were subcutaneously injected in suspension. In both cases (*i.e.*, implantation and injection), there was only a localized and transitory acute inflammatory reaction, without affecting the distal organs. Therefore, both the nanocomposites and the magnetic engineered tissues showed good *in vivo* biocompatibility. After 21 days, the nanocomposites and the constructs were not fully reabsorbed and still maintained their magnetic response. Remarkably, we measured an enhancement of the artificial tissue mechanical properties when exposed to an external magnetic field. This latter result evidences the suitability of these composites for being used in the preparation of new engineered magnetic tissues whose mechanical properties can be controlled by external, non-contact, forces. Future work will focus on the functionalization of the nanocomposites for specific purposes in regenerative medicine and tissue engineering. The magnetic tissue-like constructs could be used for cartilage tissue engineering (subjected to strong mechanical forces at the joint surface) and for the generation of biodegradable, functionalized, and mechanically stable tubes for peripheral nerve repair. However, the use of these nanocomposites should not only be restricted to tissue engineering, but could also be extended to other applications such as smart magnetic materials, biosensing and bioseparation, MRI, drug delivery or hyperthermia. In addition, the inner core may provide functionalities different than those of the shell (*e.g.*, attachment of fluorescent molecules, proteins or drugs), which can be beneficial for some of these applications.

Experimental

Preparation of Poly@Mag composites

The inner cores of the nanocomposites were PolymP–H particles kindly supplied by NanoMyP® (Spain). These particles are monodisperse acrylic copolymer (methacrylic acid (MAA) and ethylene glycol dimethacrylate (EDMA)) spheres, functionalized with carboxylic groups (170 μmol COOH per g). The chemicals used in the co-precipitation reaction (iron(III) chloride 6-hydrate; iron(II) sulphate 7-hydrate; ammonium hydroxide, 28%) were purchased from Sigma-Aldrich (USA). The water used in the different steps of the syntheses was of Milli-Q quality (Millipore, France).

The experimental procedure for preparing Poly@Mag particles was as follows: 50 mg of PolymP–H particles were dispersed in 3 mL of a 0.1 M aqueous solution of NH_4OH to promote deprotonation of the particle carboxylic groups and to charge the surface of the particles negatively. After this step, solutions of $FeCl_3{\cdot}6H_2O$ and $FeSO_4{\cdot}7H_2O$ with molar ratio $[Fe^{3+}]/[Fe^{2+}] = 0.5$ were added, and the mixture was mechanically stirred. We tested different concentrations of iron ions to determine how they affected the final thickness of the magnetic layer. To allow co-precipitation of the iron hydroxides, a solution of NH_4OH (28%) was added until pH = 12 (a black precipitate appeared). The mixture was aged for 1 hour under strong mechanical stirring, followed by heating up to 95 °C to promote magnetite formation. After cooling, the black precipitate was magnetically separated and washed with distilled water until neutral pH.

Preparation of Poly@Mag@PEG composites (polyethylene glycol, PEG, coating)

To prepare Poly@Mag@PEG composites we employed the method proposed by ref. 35 which is based on the formation of an water-in-oil microemulsion. In the water phase (15 mL) we dispersed 1 g of PEG (M_w = 400, Sigma-Aldrich, USA) and 0.3 g of Poly@Mag composites and ultrasonicated the sample for 7 min. The oil phase consisted of 450 mL of *n*-hexane, 150 mL of mineral oil and 750 μL of sorbitan sesquioleate (surfactant), all from Sigma-Aldrich (USA). Both phases were then mixed by ultrasonication for 5 min. Subsequently, 150 mL of glutaraldehyde (Sigma-Aldrich, USA) were added and the sample was stirred for 2 h. The product was finally separated and washed with water and ethanol.

Physicochemical characterization of composites

Electron microscopy. We analyzed the morphology and composition of the synthesized powders by scanning (SEM)

and transmission (TEM) electron microscopy. We used AURIGA (FIB-FESEM) and LIBRA 120 PLUS microscopes respectively (both from Carl Zeiss GmbH, Germany). The average diameter of the nanocomposites was the mean value obtained by measuring particles from TEM pictures corresponding to different windows of the supporting grid. Energy-dispersive X-ray (EDX) spectroscopy was also conducted.

X-ray diffraction (XRD). The bulk crystal structure of Poly@Mag and Poly@Mag@PEG powders was analysed using a D8 Advance powder diffractometer (Bruker, USA).

Thermogravimetric analysis (TGA). The loss of weight of the composites when heated until 650 °C (heating rate of 20 °C min^{-1}) under a N_2 atmosphere was measured with a TGA/DSC1 thermogravimetric analyzer (METTLER-TOLEDO, USA).

Fourier transform infrared spectroscopy (FTIR). FTIR spectra were recorded with a FP 6200 spectrophotometer (JASCO, Japan). The samples were prepared using the KBr pellet technique.

Analysis of gravitational settling. We scanned the temporal reduction of absorbance connected to gravitational settling using a UV–vis 8500 double-beam spectrophotometer (Dinko Instruments, Spain). We used dilute samples and measured the absorbance at λ = 590 nm for 24 h.

Chemical stability analysis. We evaluated the resistance of Poly@Mag and Poly@Mag@PEG composites against acid attack by dispersing them in a 0.1 M solution of HCl (Sigma-Aldrich, USA). After 7 days we evaluated the magnetic response of the composites by placing a neodymium magnet close to the Eppendorf tubes containing the samples.

Magnetization measurements. The magnetization of the obtained powders and of the engineered magnetic tissues was measured at room temperature as a function of the magnetic field strength in a vibrating sample magnetometer VSM 4500 (EG&G Princeton Applied Research, USA).

Zeta potential measurements. We measured the surface charge of Poly@Mag@PEG nanocomposites at physiological pH (*i.e.*, pH = 7.4) using a Malvern Zetasizer (Nano ZS) instrument. We injected dilute samples into a disposable cuvette and the experiment was run at room temperature. We conducted three runs per measurement. In each of the three measurements we used freshly prepared samples.

Ethics statement

This study was approved by the Ethics Committee of the University of Granada, Granada, Spain. Each tissue donor for the culture of fibroblasts signed an informed consent form for the study. The *in vivo* characterization was performed following the European Union and Spanish Government guidelines for ethical care of animals (EU Directive no. 63/2010, RD 53/2013). *In vivo* experiments were authorized by the Ethics Committee of the University of Granada, Granada, Spain, in the framework of the research project FIS PI14-1343.

Primary cultures of oral mucosa fibroblasts

Human oral mucosa fibroblasts were used for the biocompatibility assays and the generation of magnetic bio-artificial tissue-like constructs. Cells were isolated from 10 human oral mucosa biopsies from healthy donors (School of Dental Sciences, University of Granada) following previously described procedures.[30,54,55] Once in the laboratory, the biopsies were mechanically fragmented and digested with 2 mg per mL of *Clostridium histolyticum* collagenase I (Gibco BRL Life Technologies, Karlsruhe, Germany). Fibroblasts were harvested by centrifugation and cultured with an expansion medium (EM) composed of Dulbecco's modified Eagle's medium (DMEM, Sigma Aldrich, USA) supplemented with 10% foetal calf serum (FCS) and 1% antibiotic–antimycotic cocktail solution (100 U per ml of penicillin G, 100 mg per ml of streptomycin and 0.25 mg per ml of amphotericin B; Sigma Aldrich, Steinheim, Germany). Fibroblasts were incubated at 37 °C in 5% carbon dioxide (standard culture conditions), and EM was renewed every 3 days. Fibroblasts were expanded by using trypsin (Sigma-Aldrich, Steinheim, Germany) until the third passage and used for the generation of the bio-artificial constructs.

Cytotoxicity assays

We evaluated the *ex vivo* cell cytotoxicity of Poly@Mag and Poly@Mag@PEG composites using a primary culture of human gingival fibroblasts (24 wells per sample with a cell density of 2×10^5 cells per 500 μl of DMEM). The cells were exposed to 1 vol% of either Poly@Mag or Poly@Mag@PEG composites for 24 h. In addition, cultures of fibroblasts without any magnetic composites were used as positive controls, and the cells treated with 2% Triton X-100 as the negative control according to previous studies.[30,45,54] The cell morphology was analyzed by using a phase contrast microscope (Nikon Eclipse Ti-U, Nikon, Japan) and NIS-Elements imaging software (Nikon, Japan). The cell morphology was classified into normal (elongated and spindle-shape) or affected morphology (irregular, rounded or apoptotic bodies) under each experimental condition. Nuclear membrane permeability was evaluated by the quantification of DNA release using spectrophotometry (SmartSpec™ Plus, Bio-Rad, Hercules, CA, USA) at λ = 260–280 nm. Finally, cell proliferation and viability were measured by using the water-soluble tetrazolium salt-1 (WST-1) colorimetric assay (Cell Proliferation Reagent WST-1, Roche Diagnostics). WST-1 is a tetrazolium dye containing an electron coupling reagent that is cleaved by the mitochondrial dehydrogenase enzyme to a formazan dye. The reaction directly correlates with the number of metabolically active proliferating cells and can serve as a marker of cell viability and cell proliferation.

We report here the mean values ± standard deviations of 8 independent experiments for each experimental group and each analysis. The Kruskal–Wallis test was used to identify statistical differences among the study groups, and the Mann–Whitney test was used to identify significant differences between two groups. Values of p less than 0.05 were considered statistically significant in two-tailed tests.

Preparation of engineered magnetic tissues

The artificial magnetic tissues were generated based on the use of fibrin-agarose hydrogels following a previously reported protocol.[45] Briefly, we used 3.8 mL of human plasma (obtained from blood donors of the Health System Biobank of Granada, Spain) and added 1 million of oral mucosa fibroblasts resuspended in 0.625 mL of DMEM together with 75 μL of a solution of tranexamic acid at a concentration of 0.1 g mL^{-1} (final concentration of tranexamic acid in the biomaterial was 1.5 mg mL^{-1}). Tranexamic acid is an anti-fibrinolytic agent that prevents scaffold degradation. Afterwards, we added concentrated suspensions of Poly@Mag or Poly@Mag@PEG particles (previously sterilized by dispersion in 70% ethanol for 12 h) in DMEM to obtain a final concentration of composites in the scaffold of approximately 1.1 vol%. Subsequently, we added 0.25 mL of a mixture of type VII agarose (molecular weight 120 000 g mol^{-1}, Sigma Aldrich, USA) in PBS (0.02 g mL^{-1}, Sigma-Aldrich, Steinheim, Germany) obtaining a 0.1% final agarose concentration. Finally, we added 0.25 mL of 2% $CaCl_2$ (Sigma Aldrich, USA) to the mixture to promote polymerization of fibrin. The final solution was distributed in 6-well cell culture clusters (5 mL in each) and kept at 37 °C until complete gelation. We applied a vertical magnetic field (36 kA m^{-1}) during the first 5 minutes of gelation with a coil. After 2 hours we added EM to the constructs, and they were kept under standard culture conditions for 24 h.

Structural analysis of the tissue substitutes

We analyzed the structure of magnetic tissue substitutes by scanning electron microscopy (SEM). For this purpose, we fixed the artificial tissues with 2.5% glutaraldehyde solution and postfixed them in 1% osmium tetroxide for 90 min. Fixed samples were dehydrated at increasing concentrations of acetone, critical point-dried, mounted on aluminum stubs, and sputter-coated with gold according to routine procedures.

Cell viability of the tissue substitutes

We evaluated cell cytotoxicity by analyzing the intracellular esterase activity and the integrity of the plasma and nuclear membranes. For this purpose, we employed the LIVE/DEAD™ (L/D) assay (Viability/Cytotoxicity kit; Molecular Probes, UK) following the manufacturer's guidelines. This method contains Calcein-AM, which is metabolically modified by living cells that emit green fluorescence, and ethidium homodimer-1, which binds to the nuclei of dead cells emitting red fluorescence. After 24 h of culture, small samples from each construct were harvested, washed with PBS and incubated with the LIVE/DEAD™ solution for 30 minutes. All images were obtained and analyzed with a Nikon Eclipse 90i light and fluorescence microscope (Nikon, Japan).

Histological analyses of the tissue substitutes

After 24 h of cell culture, all samples were fixed in 10% buffered formalin for 24 h, dehydrated and embedded in paraffin. We then cut the tissues in sections of 5 μm of thickness. Histological sections were dewaxed, hydrated and stained with hematoxylin–eosin (H&E) for morphological evaluation. For the specific histochemical identification of the magnetic nanocomposites (*i.e.*, identification of ferric iron), the sections were stained with Perl's histochemical method (PERLS) (Prussian blue reaction).[56] In order to obtain an overview of the tissue, Perl's method was slightly contrasted with H&E. We also studied the active proliferation of fibroblasts by identification of the proliferating cell nuclear antigen (PCNA) by indirect immunohistochemistry as previously described.[57,58] Briefly, for immunohistochemistry, the tissue sections were dewaxed, hydrated and pretreated for antigen unmasking (citrate buffer pH = 6). Endogenous peroxidase activity was blocked with 3% (v/v) H_2O_2 in 0.1 M PBS, and the nonspecific binding of the primary antibody was blocked using casein solution (Vector, Burlingame, CA, USA). After that, the sections were incubated with the primary antibody Mouse anti-PCNA (clone PC10, Sigma Aldrich, Steinheim, Germany) 1 : 1000 in PBS tween-20 for 1 hour at room temperature. Sections were abundantly rinsed with PBS and then incubated with a Horse anti-mouse IgG conjugated with peroxidase (Vector, Burlingame, CA, USA). Finally, the antigen-antibody reaction was visualized with diaminobenzidine (DAB) (Vector, Burlingame, CA, USA) and contrasted with Mayer hematoxylin. In addition, the primary antibody was omitted in parallel slides as a technical negative control.

Rheological characterization of engineered magnetic tissues

We measured the mechanical properties of tissue substitutes at 37 °C using a Haake MARS III (Thermo Fisher Scientific, USA) controlled stress rheometer. We employed a measuring set of non-magnetic parallel plates (diameter of 3.5 cm) with rough surfaces to avoid wall slip. We applied a vertical magnetic field (*i.e.*, in the direction of the rheometer axis) using a homemade coil. The magnetic field was switched on 1 minute before each test. We placed the engineered tissues on the lower plate of the rheometer and squeezed them with the upper plate until a fixed gap of 300 μm.

We conducted two types of oscillatory shear tests. (i) Amplitude sweep tests: we fixed the frequency, f = 1 Hz, of the oscillatory strain, $\gamma = \gamma_0 \cos(2\pi f t)$ and increased the strain amplitude, γ_0, in a logarithmic ramp. The sinusoidal strain at each step was applied over 8 periods of oscillations. We recorded the resulting viscoelastic moduli (*i.e.*, the storage, G', and loss, G'', moduli) over the last 5 periods to discard transients. (ii) Frequency sweep tests: we fixed γ_0 at a value belonging to the viscoelastic linear region (*i.e.*, the region for which the viscoelastic moduli are independent of γ_0) and varied f. Again, we maintained the oscillatory strain for 8 periods and recorded the last 5. The obtained values for all the quantities in this work are the average of at least 3 repetitions.

In vivo evaluation of Poly@Mag@PEG composites and of the engineered magnetic tissues

Laboratory animals and experimental groups. For the *in vivo* assays of this work, 9-week-old male mice (*Mus Musculus*) were

provided by and maintained in the Experimental Unit of the University Hospital "Virgen de las Nieves" (Granada, Spain). The animals were deeply anaesthetized by intraperitoneal injection of a mixture of acepromizine (Calmo-Neosan®, 0.001 mg per g of weight of the animal) and ketamine (Imalgene 1000®, 0.15 mg per g of weight of the animal) after subcutaneous administration of atropine. The 27 provided animals were randomly assigned to the following three experimental groups (n = 9 in each):

(i) *in vivo* kinetic evaluation of Poly@Mag@PEG nanocomposites (S-PMPc). We evaluated the time-dependent biodistribution and biocompatibility of the Poly@Mag@PEG composites by subcutaneously injecting 500 μl of a sterile physiological suspension of the composites of concentration 11 mg mL^{-1} in the interscapulum of each mouse.

(ii) *In vivo* kinetic evaluation of engineered magnetic tissue (FA-PMPc). We evaluated the time-dependent biocompatibility of the engineered magnetic tissues by a subcutaneous implantation of a 500 μl construct (concentration of 11 mg mL^{-1}) in the interscapulum.

(iii) Control group (CTR) of healthy animals without any surgical intervention.

After injection or subcutaneous implantation of the constructs, all the animals were housed in a temperature-controlled room (21 ± 1 °C), provided with a 12 h light/dark cycle and *ad libitum* access to tap water and standard mice chow.

The *in vivo* histological biocompatibility was studied after 7, 14 and 21 days (3 mice of each group were analyzed each week, n = 3). Animals of each experimental group were euthanized by cervical dislocation and the interscapulum (skin with hypodermis), liver, kidneys, spleen and lungs were harvested for tissue processing and histological analyses.

Histological analyses. All samples were fixed in 10% buffered formalin for 24 h, dehydrated and embedded in paraffin and divided into sections of 5 μm of thickness. Histological sections were dewaxed, hydrated and stained with hematoxylin–eosin (H&E) for morphological evaluation and/or pathological evaluations. All the samples were stained using the picrosirius method which is highly specific for the evaluation of the collagen extracellular matrix.[59] In addition, we used the periodic acid-Schiff (PAS) histochemical method to evaluate the glycogen content of the liver (indicator of the normal function of this organ), the basal membrane of the kidneys (indicator of the normal structure of these organs) and the basal membrane and reticular fibers of the other tissues and organs. For the identification of Poly@Mag@PEG nanocomposites, all the tissues and organs were stained with Perls' method (described above).

Evaluation of the magnetic response of organ samples. We took samples from the area of injection/implantation, spleen, liver, lungs and kidneys and evaluated their magnetic response to identify the presence of Poly@Mag@PEG composites. For this purpose, we placed the samples near a neodymium magnet providing a magnetic field gradient of 10 mT mm^{-1} and a maximum field of 470 mT, and observed the magnetic field-induced migration of the composites towards the areas of stronger field.

Acknowledgements

This study was supported by projects FIS2013-41821-R and FISPI14-1343 (Plan Nacional de Investigación Científica, Desarrollo e Innovación Tecnológica, Ministerio de Economía y Competitividad, Spain, co-funded by ERDF, European Union) and project PI-0653-2013 (Fundación Pública Andaluza Progreso y Salud, Consejería de Salud, Junta de Andalucía, Spain). L.R.-A acknowledges financial support from the University of Granada (Contratos Puente and Fortalecimiento de Doctores programs). The authors are also grateful to NanoMyP® (Spain) for providing PolymP–H particles and for helpful discussion, and to Amalia de la Rosa Romero and Concepción López Rodríguez for their technical assistance and care of the experimental animals used in this study (Experimental Unit of the University Hospital Virgen de las Nieves, Granada).

References

1 G. Jinhao, G. Hongwei and X. Bing, *Acc. Chem. Res.*, 2009, **42**, 1097.
2 K. Chatterjee, S. Sarkar, K. Jagajjanani Rao and S. Paria, *Adv. Colloid Interface Sci.*, 2014, **209**, 8.
3 P. Hu, J. V. Morabito and C.-K. Tsung, *ACS Catal.*, 2014, **4**, 4409.
4 S. Thatai, P. Khurana, J. Boken, S. Prasad and D. Kumar, *Microchem. J.*, 2014, **116**, 62.
5 M. R. Kim, Z. Xu, G. Chen and D. Ma, *Chem. – Eur. J.*, 2014, **20**, 11256.
6 V. Salgueiriño-Maceira and M. A. Correa-Duarte, *Adv. Mater.*, 2007, **19**, 4131.
7 S. Behrens, *Nanoscale*, 2011, **3**, 877.
8 M. Colombo, S. Carregal-Romero, M. F. Casula, L. Gutierrez, M. P. Morales, I. B. Böhm, J. T. Heverhagen, D. Prosperi and W. J. Parak, *Chem. Soc. Rev.*, 2012, **41**, 4306.
9 J. K. Oh and J. M. Park, *Prog. Polym. Sci.*, 2011, **36**, 168.
10 M. Bañobre-López, Y. Piñeiro-Redondo, R. de Santis, A. Gloria, L. Ambrosion, A. Tampieri, V. Dediu and J. Rivas, *J. Appl. Phys.*, 2011, **109**, 07B313.
11 N. Bock, A. Riminucci, C. Dionigi, A. Russo, A. Tampieri, E. Landi, V. A. Goranov, M. Marcacci and V. Dediu, *Acta Biomater.*, 2010, **6**, 786.
12 B. Das, M. Mandal, A. Upadhyay, P. Chattopadhyay and N. Karak, *Biomed. Mater.*, 2013, **8**, 035003.
13 A. Gloria, T. Russo, U. D'Amora, S. Zeppetelli, T. D'Alesssandro, M. Sandri, M. Bañobre-Lopez, Y. Piñeiro-Redondo, M. Uhlarz, A. Tampieri, J. Rivas, T. Herrmannsdördfer, V. A. Dediu, L. Ambrosio and R. De Santis, *J. R. Soc., Interface*, 2013, **10**, 20120833.
14 H. Hu, W. Jiang, F. Lan, X. Zeng, S. Man, Y. Wu and Z. Gu, *RSC Adv.*, 2013, **3**, 879.

15 K. Lai, W. Jiang, J. Z. Tang, Y. Wu, B. He, G. Wang and W. Gu, *RSC Adv.*, 2012, **2**, 13007.
16 H. Liu, C. Wang, Q. Gao, X. Liu and Z. Tong, *Acta Biomater.*, 2010, **6**, 275.
17 S. Panseri, C. Cunha, T. D'Alessandro, M. Sandri, G. Giavaresi, M. Marcacci, C. T. Hung and A. Tampieri, *J. Nanobiotechnol.*, 2012, **10**, 32.
18 H. Skaat, O. Ziv-Polat, A. Shahar, D. Last, Y. Mardor and S. Margel, *Adv. Healthcare Mater.*, 2012, **1**, 168.
19 A. Tampieri, E. Landi, F. Valentini, M. Sandri, T. D'Alessandro, V. Dediu and M. Marcacci, *Nanotechnology*, 2011, **22**, 015104.
20 X. B. Zeng, H. Hu, L. Q. Xie, F. Lan, W. Jiang, Y. Wu and Z. W. Gu, *Int. J. Nanomed.*, 2012, **7**, 3365.
21 Y. Zhu, F. Shang, B. Li, Y. Dong, Y. Liu, M. R. Lohe, N. Hanagata and S. Kaskel, *J. Mater. Chem. B*, 2013, **1**, 1279.
22 O. Ziv-Polat, H. Skaat, A. Shahar and S. Margel, *Int. J. Nanomed.*, 2012, **7**, 1259.
23 S.-H. Hu, T.-Y. Liu, C.-H. Tsai and S.-Y. Chen, *J. Magn. Magn. Mater.*, 2007, **310**, 2871.
24 A. Tampieri, T. D'Alessandro, M. Sandri, S. Sprio, E. Landi, L. Bertinetti, S. Panseri, G. Pepponi, J. Goettlicher, M. Bañobre-Lopez and J. Rivas, *Acta Biomater.*, 2012, **8**, 843.
25 N. H. A. Ngadiman, A. Idris, M. Irfan, D. Kurniawan, N. M. Yusof and R. Nasiri, *J. Mech. Behav. Biomed. Mater.*, 2015, **49**, 90.
26 M. R. Dzamukova, E. A. Naumenko, E. V. Rozhina, A. A. Trifonov and R. F. Fakhrullin, *Nano Res.*, 2015, 1.
27 G. Bossis, O. Volkova, S. Lacis and A. Meunier, *Lect. Notes Phys.*, 2002, **594**, 201.
28 J. D. Carlson and M. R. Jolly, *Mechatronics*, 2000, **10**, 555.
29 J. de Vicente, D. J. Klingenberg and R. Hidalgo-Alvarez, *Soft Matter*, 2011, **7**, 3701.
30 M. T. Lopez-Lopez, G. Scionti, A. C. Oliveira, J. D. G. Duran, A. Campos, M. Alaminos and I. A. Rodriguez, *PLoS One*, 2015, **10**, e0133878.
31 L. Rodriguez-Arco, M. T. Lopez-Lopez, P. Kuzhir, G. Bossis and J. D. G. Durán, *ACS Appl. Mater. Interfaces*, 2013, **5**, 12143.
32 R. Petros and J. M. DeSimone, *Nat. Rev. Drug Discovery*, 2010, **9**, 615.
33 M. Arruebo, M. Galan, N. Navascues, C. Tellez, C. Marquina, M. R. Ibarra and J. Santamaria, *Chem. Mater.*, 2006, **18**, 1911.
34 H. Otsuka, Y. Nagasaki and K. Kataoka, *Adv. Drug Delivery Rev.*, 2012, **64**, 246.
35 J. Chatterjee, M. Bettge, Y. Haik and C. J. Chen, *J. Magn. Magn. Mater.*, 2005, **293**, 303.
36 P. Govindaiah, S. J. Lee, J. H. Kim and I. W. Cheong, *Polymer*, 2011, **52**, 5058.
37 J. Rubio-Retama, N. E. Zafeiropoulos, C. Serafinelli, R. Rojas-Reyna, B. Vois, E. Lopez Cabarcos and M. Stamm, *Langmuir*, 2007, **23**, 10280.
38 A. Pich, S. Bhattacharya and H.-J. P. Adler, *Polymer*, 2005, **46**, 1077.
39 V. Cabuil, in *Encyclopedia of Surface and Colloid Science*, ed. P. Somasundaran, Taylor&Francis, New York, 2006.
40 M. E. Evans and F. Heller, *Environmental Magnetism. Principles and Application of Enviromagnetics*, ed. F. Cynar, Elsevier Science, New York, 2003.
41 L. D. Landau and E. M. Lifshitz, *Electrodynamics of Continuous Media*, Pergamon, New York, 1984.
42 K. W. Yu and K. P. Yuen, *J. Phys.: Condens. Matter*, 1996, **8**, 11327.
43 S. A. Gómez-Lopera, R. C. Plaza and A. V. Delgado, *J. Colloid Interface Sci.*, 2001, **240**, 40.
44 S. A. Gómez-Lopera, J. L. Arias, V. Gallardo and A. V. Delgado, *Langmuir*, 2006, **22**, 2816.
45 M. Alaminos, M. C. Sanchez-Quevedo, J. I. Muñoz-Avila, D. Serrano, S. Medialdea, I. Carreras and A. Campos, *Invest. Ophthalmol. Visual Sci.*, 2006, **47**, 3311.
46 I. A. Rodriguez, M. T. Lopez-Lopez, A. C. X. Oliveira, M. C. Sanchez-Quevedo, A. Campos, M. Alaminos and J. D. G. Duran, *J. Tissue Eng. Regener. Med.*, 2012, **6**, 636.
47 G. Scionti, M. Moral, M. Toledano, R. Osorio, J. D. G. Durán, M. Alaminos, A. Campos and M. T. López-López, *J. Biomed. Mater. Res., Part A*, 2014, **102**, 2573.
48 J. M. Viñuela-Prieto, M. C. Sánchez-Quevedo, C. A. Alfonso-Rodríguez, A. C. Oliveira, G. Scionti, M. A. Martín-Piedra, G. Moreu, A. Campos, M. Alaminos and I. Garzón, *J. Periodontal Res.*, 2015, **50**, 658.
49 G. Hudry-Clergeon, G. Marguerie, L. Pouit and M. Suscillon, *Thromb. Res.*, 1975, **6**, 533.
50 U. Wattendorf and H. P. Merkle, *J. Pharm. Sci.*, 2008, **97**, 4655.
51 R. G. Larson, in *The Structure and Rheology of Complex Fluids*, ed. K. E. Gubins, Oxford University Press, New York, 1999.
52 S. Kasapis in *Modern Biopolymer Science. Bridging the Divide between Fundamental Treatise and Industrial Application*, ed. S. Kasapis, I. T. Norton and J. B. Ubbink, Elsevier, Oxford, 2009.
53 S. Rose, A. Prevoteau, P. Elziere, D. Hourder, A. Marcellan and L. Leibler, *Nature*, 2014, **505**, 382.
54 I. A. Rodriguez, G. Lopez-Gonzalez, M. A. Rodriguez, F. Campos-Sanchez and M. Alaminos, *J. Adhes. Dent.*, 2011, **13**, 375.
55 S. San Martin, M. Alaminos, T. M. T. Zorn, I. Garzón and I. A. Rodriguez, *J. Tissue Eng. Regener. Med.*, 2013, **7**, 10.
56 J. A. Kiernan, in *Histological and Histochemical Methods: Theory and Practice*, ed. D. J. Dries, Scion, Oxfordshire, 2008.
57 M. A. Rodriguez, M. T. Lopez-Lopez, J. D. Duran, M. Alaminos, A. Campos and I. A. Rodriguez, *Cryobiology*, 2013, **67**, 355.
58 V. Carriel, G. Scionti, F. Campos, O. Roda, B. Castro, M. Cornelissen, I. Garzon and M. Alaminos, *J. Tissue Eng. Regener. Med.*, 2015, DOI: 10.1002/term.2039.
59 V. Carriel, I. Garzón, M. Alaminos and A. Campos, *Histochem. Cell Biol.*, 2011, **136**, 709.

